Journal of Thrombosis and Haemostasis, **8**: 1044–1053 DOI: 10.1111/j.1538-7836.2010.03826.x

ORIGINAL ARTICLE

Dynamical view of membrane binding and complex formation of human factor VIIa and tissue factor

Y. Z. OHKUBO,*† J. H. MORRISSEY†‡ and E. TAJKHORSHID*†‡§

Beckman Institute for Advanced Science and Technology, University of Illinois, Urbana; †Department of Biochemistry, University of Illinois, Urbana; ‡College of Medicine, University of Illinois, Urbana; and §Center for Biophysics and Computational Biology, University of Illinois, Urbana, IL, USA

To cite this article: Ohkubo YZ, Morrissey JH, Tajkhorshid E. Dynamical view of membrane binding and complex formation of human factor VIIa and tissue factor. *J Thromb Haemost* 2010; **8**: 1044–53.

Summary. *Background:* The molecular mechanism of enhancement of the enzymatic activity of factor VIIa by tissue factor (TF) is not fully understood, primarily because of the lack of atomic models for the membrane-bound form of the TF–FVIIa complex. *Objectives:* To construct the first membrane-bound model of the TF–FVIIa complex, and to investigate the dynamics of the complex in solution and on the surface of anionic membranes by using large-scale molecular dynamics (MD) simulations in full atomic detail. *Methods:* Membrane-bound models of the TF–FVIIa complex and the individual factors were constructed and subjected to MD simulations, in order to characterize protein–protein and protein–lipid interactions, and to investigate the dynamics of TF and FVIIa. *Results:* The MD trajectories reveal that isolated FVIIa undergoes large structural fluctuation, primarily due to the hinge motions between its domains, whereas soluble TF (sTF) is structurally stable. Upon complex formation, sTF restricts the motion of FVIIa significantly. The results also show that, in the membrane-bound form, sTF directly interacts with the lipid headgroups, even in the absence of FVIIa. *Conclusion:* The first atomic models of membrane-bound sTF–FVIIa, FVIIa and sTF are presented, revealing that sTF forms direct contacts with the lipids, both in the isolated form and in complex with FVIIa. The main effect of sTF binding to FVIIa is spatial stabilization of the catalytic site of FVIIa, which ensures optimal interaction with the substrate, FX.

Keywords: coagulation cascade, factor VIIa, GLA domain, molecular dynamics simulation, protein–protein interaction, tissue factor.

Correspondence: Emad Tajkhorshid, University of Illinois at Urbana-Champaign, Beckman Institute, 405 N. Mathews, Urbana, IL 61801, USA.
Tel: + 1 217 244 6914; fax: + 1 217 244 6078.
E-mail: emad@life.uiuc.edu

Received 9 January 2010, accepted 16 February 2010

Introduction

The rate of the enzymatic activity of proteolytic reactions involved in the blood clotting cascade [1–3] is enhanced by several orders of magnitude upon binding of the coagulation factors to anionic regions of the cellular membrane, especially regions that are rich in phosphatidylserine (PS). For vitamin K-dependent coagulation factors, the key step of membrane binding hinges on the GLA domain, a major membrane-anchoring domain mediating the binding of coagulants to the surface of the membrane in a Ca^{2+}-dependent manner (we use 'GLA' for this Gla-rich domain, and 'Gla' to refer to γ-carboxyglutamic acid residues). Vitamin K-dependent coagulation proteins, namely factor VII [4–6], FIX [7,8], FX [9,10], and prothrombin [11–13], as well as the anticoagulant protein C [14] and its cofactor protein S [15], and protein Z, share this membrane-anchoring domain.

One of the initial steps along the extrinsic pathway is the activation of FX to FXa, catalyzed through the formation of the ternary complex of activated FVII (FVIIa) (the proteolytic enzyme), tissue factor (TF) (the cofactor), and FX (the substrate). FVIIa is one of the essential serine proteases in the coagulation cascade. In order to gain full catalytic activity, FVIIa needs to bind to its cofactor, TF, forming the TF–FVIIa complex (the extrinsic FXase; Fig. 1). The catalytic efficiency (k_{cat}/K_m) of FX hydrolysis by FVIIa is increased by 10^6–10^7-fold when FVIIa is associated with TF [16]. TF is composed of four domains: a cytoplasmic domain, which appears not to be needed for the coagulation function of this factor [17,18]; a transmembrane domain, which anchors TF in the membrane (presumably a single α-helix, for which no structure has yet been reported); a linker region connecting the transmembrane and extracellular domains; and the extracellular domain (major functional domain). The extracellular domain of TF, often referred to as soluble TF (sTF; used throughout this article to distinguish this domain from the entire TF), has been expressed separately and shown to account for the activity of this factor [17].

© 2010 International Society on Thrombosis and Haemostasis

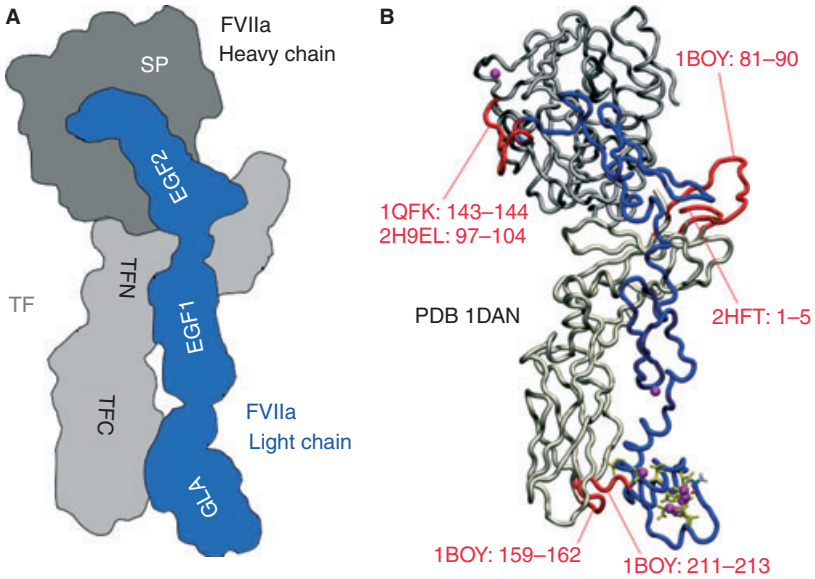


Fig. 1. Architectural overview and structural modeling of the soluble tissue factor (sTF)–FVIIa complex. (A) Schematic representation of the complex. sTF (shown in light gray) consists of N-terminal (residues 1–106) and C-terminal (residues 107–213) fibronectin type III domains (labeled TFN and TFC, respectively). FVIIa consists of four domains: the serine protease (SP) domain, which forms the heavy chain (dark gray), the GLA domain (GLA; residues 1–46), the epidermal growth factor (EGF)-like domain 1 (EGF1; residues 47–83), and the EGF-like domain 2 (EGF2; residues 87–128). The last three domains form the light chain (blue). (B) Construction of the complete model of the sTF–FVIIa complex, starting from the Protein Data Bank (PDB) entry 1DAN [4]. The backbones of sTF (light gray), SP (dark gray), GLA, EGF1 and EGF2 (blue) are drawn in tube representation. The Gla side chains of the GLA domain are drawn in a yellow stick representation, and FVIIa-bound calcium ions are drawn as purple spheres. Missing loops (red) were constructed using other PDB entries, with the residue numbers specified.

A number of studies have proposed different mechanisms by which the association with TF might affect the activity of FVIIa. Analysis of the binding of FVIIa and TF in solution indicated that the GLA domain of FVIIa might play roles other than membrane binding; it was found that the GLA domain is not only important for the formation of a more stable TF–FVIIa complex, but also contributes to an extended substrate recognition region [19,20]. Other biochemical studies found evidence that TF can also directly induce alteration of the FVIIa catalytic activity through an allosteric mechanism that is independent of the supporting membrane [16].

The structure of the sTF–FVIIa complex has been determined crystallographically [4]. Under physiologic conditions, sTF is anchored to the membrane with a single transmembrane segment, which is connected to sTF by a short (six amino acid) linker. Owing to the structural flexibility of the linker, the transmembrane segment is most likely decoupled conformationally from sTF, and thus is not expected to be important in controlling the relative orientation of sTF on the membrane [18]. Additionally, direct interaction between sTF and the membrane has been suspected to account for the observation that removal of the GLA domain from FVIIa has little effect on its active site positioning relative to the membrane in the TF–FVII complex, suggesting that sTF is sufficiently well oriented on the membrane (even in the absence of its membrane-anchoring helix) to hold FVIIa in an optimal (vertical) orientation on the surface of the membrane [21,22]. However, the nature of such direct interactions between sTF (or TF) and the membrane, as well as that between (s)TF and FVIIa on the surface of the membrane, is completely unknown [23], although several sTF sites that are directly involved in the binding of the substrates (FIX, FX, and FVII itself) have been reported [24–28].

Several modeling and simulation studies have investigated various aspects of the sTF–FVIIa complex and how they might contribute to the increased enzymatic activity of FVIIa [29–33]. However, the role of the membrane was never addressed in any of these studies. Docking and molecular dynamics (MD) studies of the sTF–FVIIa–FXa ternary complex in solution reported that the C-terminal region of the GLA domain of FVIIa interacts with that of FXa in the complex [32]. Another MD study, corroborated by hydrogen exchange experiments, reported sTF-induced structural change in the serine protease domain of FVIIa [33]. The effect of lipid molecules, however, was again not taken into account in these studies, as the simulations were conducted in solution.

Here, we sought to characterize the dynamic and structural consequences of complex formation between sTF and FVIIa, as well as the modes of interactions of these proteins, particularly sTF, with the membranes. We employed MD simulations of the sTF–FVIIa complex and individual monomers to investigate the changes in their dynamic behavior and to characterize protein–protein and protein–lipid interactions upon complex formation, and how they might result in increased enzymatic activity of FVIIa.

© 2010 International Society on Thrombosis and Haemostasis

Materials and methods

Modeling of sTF and FVIIa

The coordinates of the complex of human sTF and FVIIa with seven bound calcium ions were taken from Protein Data Bank (PDB) entry 1DAN [4]. Missing loop regions of sTF were modeled using the corresponding residues from other PDB entries of isolated sTF, that is, 1BOY [34] and 2HFT [35] (Fig. 1B). The missing C-terminal residues 143 and 144 of chain L of FVIIa were modeled on the basis of the corresponding residues from another PDB entry of isolated FVIIa, 1QFK [36], and residues 145–152 from a segment of FXa, PDB 2H9E [37] (residues 97–104 of chain L), which has the highest BLAST [38] score among the available structures in the PDB. Hydrogen atoms were added, and the N-terminus and C-terminus were modified so that they had charged amino and carboxy groups, respectively.

System preparation

The modeled proteins were solvated in a water box that provided a minimum padding of 12 Å on each side. The system was then neutralized by randomly replacing water molecules in the bulk with sodium and chloride ions to achieve a final ion concentration of 250 mM. To remove any steric clashes that might have been introduced during the modeling phase, the solvated, neutralized systems were subjected to several cycles of relaxation. Each cycle included an energy minimization step followed by a short (10-ps) MD simulation, which provides a more efficient way of removing possible steric clashes. In the first cycle, only the modeled parts were allowed to move, with the rest of the system constrained; in subsequent cycles, the constraints applied to the system were gradually removed, with the last cycle treating the entire model without any constraints.

A more detailed description of the procedures used in system preparation is provided in Data S1. In short, to construct membrane models, the sTF–FVIIa complex and isolated FVIIa were superimposed, using their respective GLA domains, on the membrane-bound model of the GLA domain of FVII [39,40]. The membrane-bound model of isolated sTF was prepared by removing FVIIa from the system of sTF–FVIIa on the 1,2-dioleoyl-*sn*-glycero-3-phosphoserine (DOPS) membrane. A pure DOPS lipid bilayer was employed in order to maximize the sampling of various modes of interaction between the proteins and PS headgroups during the limited time scales accessible to MD simulations. These membrane-bound models were then solvated and neutralized in the same manner as the solution systems. All of the systems were then simulated using equilibrium MD for 50–90 ns (Table 1).

Simulation procedures

All of the simulations were performed using NAMD 2.6 [41] with the CHARMM27 force field parameters [42], and the TIP3P model for water [43]. Langevin dynamics with a damping coefficient of 1 ps^{-1} was used to maintain the temperature at 310 K. The Langevin piston Nosé–Hoover method [44,45] was employed to maintain the pressure at 1 atm. The particle mesh Ewald (PME) method [46], with a grid density slightly finer than 1 $Å^{-3}$, was used to calculate long-range electrostatic forces without truncation. The cut-off for van der Waals interaction was set at 12 Å. Integration time steps were set at 1, 1 and 2 fs for bonded, non-bonded and PME calculations, respectively. The solution systems were simulated in the *NPT* ensemble (constant pressure and temperature), and the membrane-bound systems in the NP_nTA ensemble (constant membrane-normal pressure, P_n, temperature, and membrane area).

Table 1 The simulation systems reported in this study

System	Environment	Time (ns)
sTF	Solution	60
FVIIa	Solution	60
sTF	Membrane	50
FVIIa	Membrane	80
sTF–FVIIa	Membrane	90

sTF, soluble tissue factor.

Results and Discussion

Locking effect of sTF on the rocking motion of FVIIa

The calculated root mean square deviations (RMSDs) for sTF, FVIIa and their complex in different simulations are provided in Table 2. In order to highlight the relative motions of the individual domains of these proteins and to contrast the high flexibility of the protein with the observed structural stability of the composing domains, we also calculated RMSDs after superposition of the trajectories using individual domains (Table 3). The dynamics of FVIIa and sTF captured during the simulations of different systems are also displayed in Fig. 2, in which instantaneous conformations are superimposed using the Cα atoms of individual domains: GLA, epidermal growth factor (EGF)1, EGF2 or serine protease (SP) for FVIIa; and TF N-terminal fibronectin type III domain (TFN) or TF C-terminal fibronectin type III domain (TFC) for sTF (see also Video Clip S1).

Table 2 Average Cα root mean square deviations (RMSDs) and standard deviations (in parentheses) for the entire protein(s) calculated from the simulations of individual proteins [soluble tissue factor (sTF) and FVIIa] and their complex (sTF–FVIIa)

System	Environment	Cα RMSD (Å) Mean (SD)
FVIIa	Solution	12.34 (3.91)
sTF	Solution	3.03 (0.45)
FVIIa	Membrane	7.11 (2.01)
sTF	Membrane	2.37 (0.43)
sTF–FVIIa in sTF–FVIIa	Membrane	2.94 (0.41)
FIIA in sTF–FVIIa	Membrane	2.88 (0.43)
sTF in sTF–FVIIa	Membrane	2.61 (0.45)

© 2010 International Society on Thrombosis and Haemostasis

Table 3 Cα root mean square deviations (RMSDs) of soluble tissue factor (sTF) and FVIIa aligned using the respective domains

			Aligned domain and RMSDs for all domains and the aligned domains (Å)					
System	Environment	Domain	GLA	EGF1	EGF2	SP	TFC	TFN
FVIIa	Solution	All	48.88 (14.12)	43.48 (14.11)	24.75 (8.68)	24.23 (8.55)	–	–
		Aligned	0.93 (0.17)	1.84 (0.31)	2.35 (0.47)	2.27 (0.62)	–	–
sTF	Solution	All	–	–	–	–	4.04 (0.86)	4.60 (1.43)
		Aligned	–	–	–	–	1.83 (0.24)	3.24 (0.57)
FVIIa	Membrane	All	31.83 (8.51)	35.62 (12.30)	12.63 (4.59	12.64 (4.76)	–	–
		Aligned	0.73 (0.11)	2.50 (0.34)	2.04 (0.49)	2.12 (0.53)	–	–
sTF	Membrane	All	–	–	–	–	3.15 (0.77)	3.19 (0.88)
		Aligned	–	–	–	–	1.85 (0.28)	2.35 (0.57)
FVIIa in sTF–FVIIa	Membrane	All	9.30 (4.02)	7.45 (2.39)	5.94 (1.84)	3.47 (0.66)	–	–
		Aligned	1.04 (0.22)	1.35 (0.24)	1.55 (0.22)	2.23 (0.42)	–	–
sTF in sTF–FVIIa	Membrane	All	–	–	–	–	3.36 (0.77)	3.46 (0.92)
		Aligned	–	–	–	–	1.39 (0.25)	3.04 (0.60)

EGF, epidermal growth factor; SP, serine protease; TFC, tissue factor C-terminal fibronectin type III domain; TFN, tissue factor N-terminal fibronectin type III domain. Average Cα RMSDs and standard deviations (in parentheses) calculated either for the entire molecule or for individual domains (GLA, EGF1, EGF2, SP, TFC, and TFN). In contrast to Table 2, the individual domains are used for the alignment of the snapshots in each trajectory.

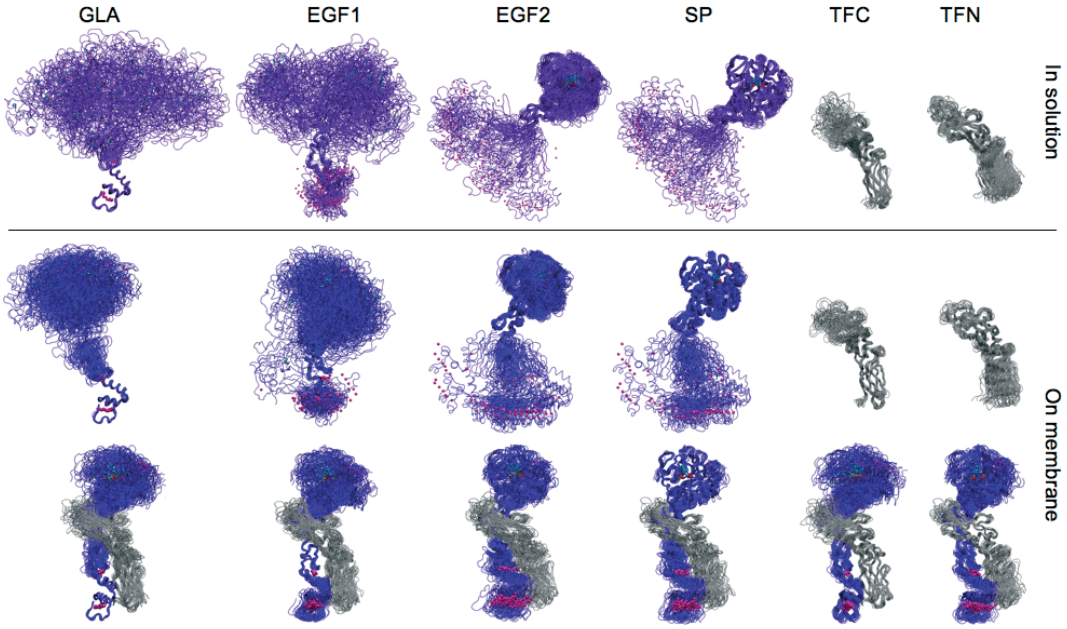


Fig. 2. Dynamics of soluble tissue factor (sTF) and FVIIa. Superimposed snapshots taken at 2-ns intervals from the simulations of sTF and FVIIa individually, as well as that of the sTF–FVIIa complex in solution or on the membrane, are shown. sTF is colored gray; FVIIa is colored purple when in solution, and blue when on the membrane. In each column, a different domain [GLA, epidermal growth factor (EGF)1, EGF2, serine protease (SP), tissue factor (TF) C-terminal fibronectin type III (TFC), or TF N-terminal fibronectin type III (TFN)] has been used for structural overlay of the snapshots, in order to depict relative movement of the domains and to emphasize that the individual domains are internally stable. FVIIa-bound calcium ions are drawn as purple spheres, and the side chains of the catalytic triad in the SP domain are drawn in stick representation (see Fig. 3 for a more detailed view).

FVIIa exhibited significant flexibility and large fluctuations both in solution and on the surface of the membrane, whereas sTF presented a stable conformation regardless of the environment or configuration. The Cα RMSDs of isolated FVIIa were over 30 Å when superimposed using the GLA or EGF1 domains, both in solution and on the membrane, whereas the corresponding RMSD values for FVIIa in the sTF–FVIIa complex were < 10 Å. This trend, which is in good agreement with the findings of an earlier MD study of isolated FVIIa and sTF–FVIIa complex in solution [29], clearly indicates that TF binding has a significant confining effect on the internal motion of FVIIa (see also Video Clip S1). The observed phenomenon is supported by experimental results indicating that TF is able to restrict large-scale internal motion of FVIIa, although the nature of the movements involved could not be characterized [47].

Interestingly, the Cα RMSDs within individual domains invariably remained small, being at most 2.5 Å for EGF1 and

© 2010 International Society on Thrombosis and Haemostasis

around 1–2 Å for other domains (Table 3). These results demonstrate that the large motion of FVIIa primarily originates from the relative displacement of its individual domains, which are each internally stable. This hinge-like (rocking) motion of FVIIa was significantly quenched upon complex formation with sTF. In other words, sTF rigidifies (or locks) FVIIa on the surface of the membrane. In comparison, the fluctuations of sTF were smaller. The Cα RMSDs for the whole sTF or for its individual domains were around 2–3 Å. The RMSDs were slightly smaller for the membrane-bound sTF than for sTF in solution, and for TFC than for TFN.

Dynamics of FVIIa on the surface of the membrane

The simulated membrane-bound systems of isolated FVIIa and the sTF–FVIIa complex reveal an important role of sTF in rigidifying FVIIa (Table 3 and Fig. 2). Both the isolated FVIIa and the sTF–FVIIa complex remained on the surface of the DOPS membrane during the simulations, exhibiting only slight changes in the orientation of the GLA domains against the membrane. However, FVIIa exhibited far larger fluctuation against the membrane in the isolated form (31.8 Å) than in complex with sTF (9.3 Å), as clearly demonstrated in Fig. 3A.

The stabilizing role of sTF is further supported by the appearance of a large-scale, soft mode of fluctuation in the time series of Cα RMSDs of FVIIa in its isolated form (Fig. 3B), although (about an order of magnitude) longer simulations would be required to fully validate this effect. The isolated FVIIa seemed to exhibit Cα RMSD fluctuations with a period of around 50 ns, whereas FVIIa in the complex exhibited smaller, faster fluctuations on the order of a few nanoseconds, suggesting that the soft motion of FVIIa had vanished on binding to sTF.

A major effect of the structural rigidification of FVIIa by sTF is the spatial confinement of the catalytic triad (CT, composed of His57, Asp102, and Ser195) in the SP domain, in terms of both its relative height and its projection onto the surface of the membrane. This effect was visualized graphically by monitoring the positions of the side chains of the CT during the simulation, revealing a wide spatial scatter of this region, particularly with respect to the membrane projection of the CT, that is, its position within the x–y plane parallel to the membrane (Fig. 4). The standard deviations of the x and y coordinates of the Ser195 Cα were ± 11.2 Å and ± 8.5 Å for isolated FVIIa, and only ± 5.5 Å and ± 6.3 Å for FVIIa in the complex (Fig. 4), indicating that the lateral fluctuation range of the CT in the sTF–FVIIa complex was restricted to about one-third of that in the isolated FVIIa. Furthermore, the CT in the complex maintained a position directly above the GLA domain and sTF, whereas in the isolated FVIIa it scattered over a wide region, mostly distant from the position above the GLA domain (Fig. 4). Combined with the rotation of the SP domain, this resulted in a totally different position and orientation of the CT in the absence of sTF. The relative position of the CT is of utmost importance for interaction with FX, which has been suggested to approach and bind the sTF–FVIIa complex from the putative exosite side of sTF (specified by a blue arrow in Fig. 4) [24–28].

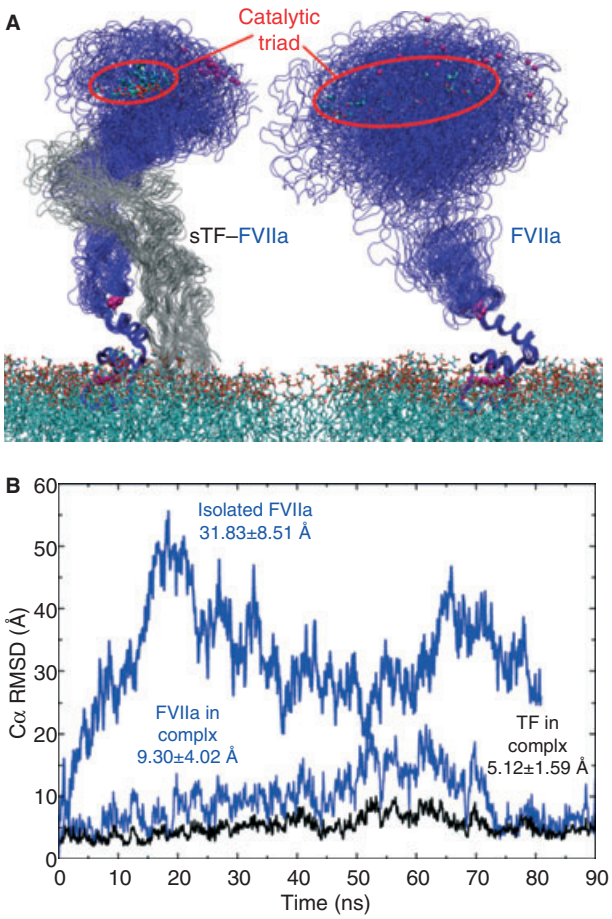


Fig. 3. Impact of soluble tissue factor (sTF) on the dynamics of FVIIa on the membrane. (A) Close-up views of the GLA-aligned snapshots taken from the simulations of the sTF–FVIIa complex (left) and isolated FVIIa (right) on the membrane. The FVIIa-bound calcium ions are drawn as purple spheres, and the catalytic triad (CT) and the 1,2-dioleoyl-*sn*-glycero-3-phosphoserine (DOPS) lipids in stick representation. Red ovals are used to indicate the range of the CT fluctuation in the two systems. (B) Time series of the Cα root mean square deviations (RMSDs) calculated for isolated FVIIa on the membrane (thick blue line), FVIIa in the sTF–FVIIa complex on the membrane (blue line), and sTF in the sTF–FVIIa complex on the membrane (black line). The average Cα RMSDs and standard deviations calculated over the entire trajectory are also indicated for all systems.

The distance between the membrane and the CT (CT height), which has been experimentally estimated [21,22], can also play an important role in determining the optimal pose of the CT for interaction with FX. The CT height is defined here as the difference between the average z-coordinate of all carboxy oxygens in the serine headgroups of the proximal lipid leaflet, which constitute the outermost layer of the DOPS bilayer [40,48], and that of the Cα atoms of the CT residues. The CT height of isolated FVIIa (85.1 ± 3.8 Å) was slightly shorter than that of FVIIa in the complex (88.1 ± 1.4 Å), and the standard deviation was larger for the former, indicating that sTF holds the SP domain in a more upright position,

© 2010 International Society on Thrombosis and Haemostasis

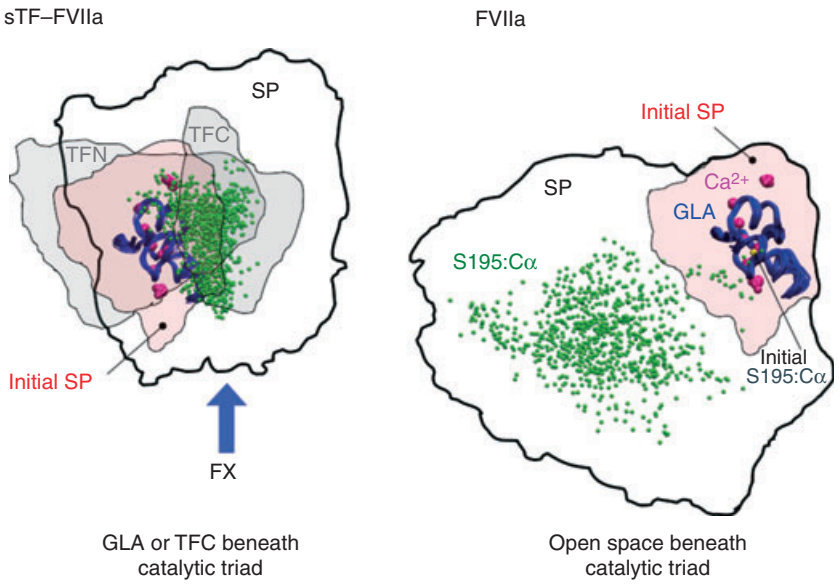


Fig. 4. The effect of soluble tissue factor (sTF) on the fluctuation of the serine protease (SP) domain of the membrane-bound FVIIa. Top view of Fig. 3A, showing the footprints (membrane projections) of various domains during the simulations of the sTF–FVIIa complex (left) and isolated FVIIa (right) on the membrane. Thick lines encompass the region in which the SP domain fluctuates in the *x*–*y* plane (parallel to the membrane). As a reference, the initial footprint of the SP domain (initial SP) is also indicated by pink shading. In the left panel, the range of tissue factor (TF) N-terminal fibronectin type III domain (TFN) and TF C-terminal fibronectin type III domain (TFC) fluctuations is indicated by gray shading. The GLA domains (used for structural alignment in both cases) are shown as blue tubes, with the bound calcium ions drawn as large purple spheres. As a measure of the spatial scatter of the catalytic triad, the position of the Cα atom of Ser195, taken from multiple frames of the trajectories, is shown as small green spheres. The initial position of this residue is drawn as a small yellow sphere, and labeled in the right panel. The putative FX-binding interface is marked with a blue arrow in the left panel.

resulting in a slightly higher position of the CT than in the isolated FVIIa. However, the extent of the effect was much smaller than the confining effect of sTF on the projected position and orientation of the SP domain, which were described above. The CT heights calculated from the simulations are in close agreement with the distances derived from fluorescence resonance energy transfer measurements [21,22], which also showed that FVIIa adopts a perpendicular orientation relative to the surface of the membrane.

Direct interaction of sTF with the membrane

During the membrane simulations, sTF maintained its membrane-bound state both in its isolated form and in the sTF–FVIIa complex, establishing direct contacts with anionic DOPS molecules through several residues located at the bottom of TFC (Fig. 5). On the basis of these results, we suggest that the transmembrane and linker regions of TF are not required for establishing direct interactions between the membrane and TF and for keeping sTF on the surface of the membrane.

Whereas the conformation of sTF remains mostly unchanged upon complex formation with FVIIa on the surface of the membrane, its orientation against the membrane changes significantly. Figure 6A shows representative snapshots of sTF on the membrane with and without FVIIa. Two angles, θ_{NC}, between TFN and TFC, and θ_{CM}, between the membrane and sTF (see Fig. 6 for the exact definitions), were used to define the

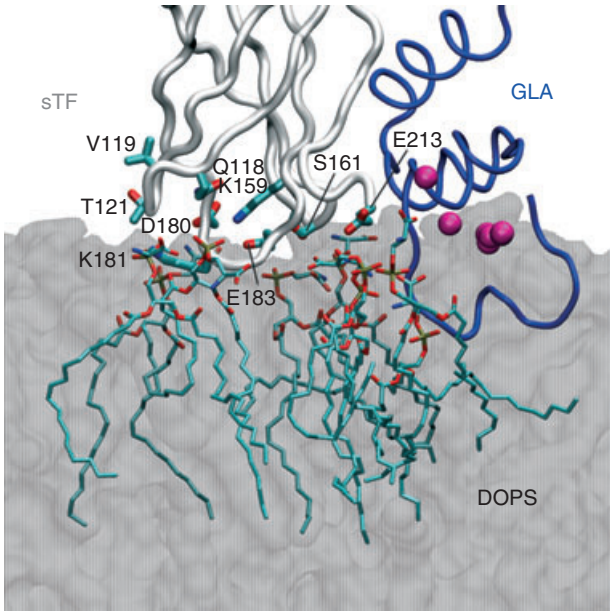


Fig. 5. Direct interaction of soluble tissue factor (sTF) with the membrane. A snapshot of the sTF–FVIIa complex on the membrane is shown, in which direct contacts of sTF with several 1,2-dioleoyl-*sn*-glycero-3-phosphoserine (DOPS) molecules in the membrane are highlighted. DOPS molecules and the side chains of sTF that are within 5 Å are drawn in stick representation. The membrane is drawn using transparent gray shading. The backbone of the GLA domain of FVIIa and sTF are drawn in blue and light gray tube representations, respectively. The GLA domain-bound calcium ions are drawn as purple spheres (not all seven ions are distinguishable in this view).

© 2010 International Society on Thrombosis and Haemostasis

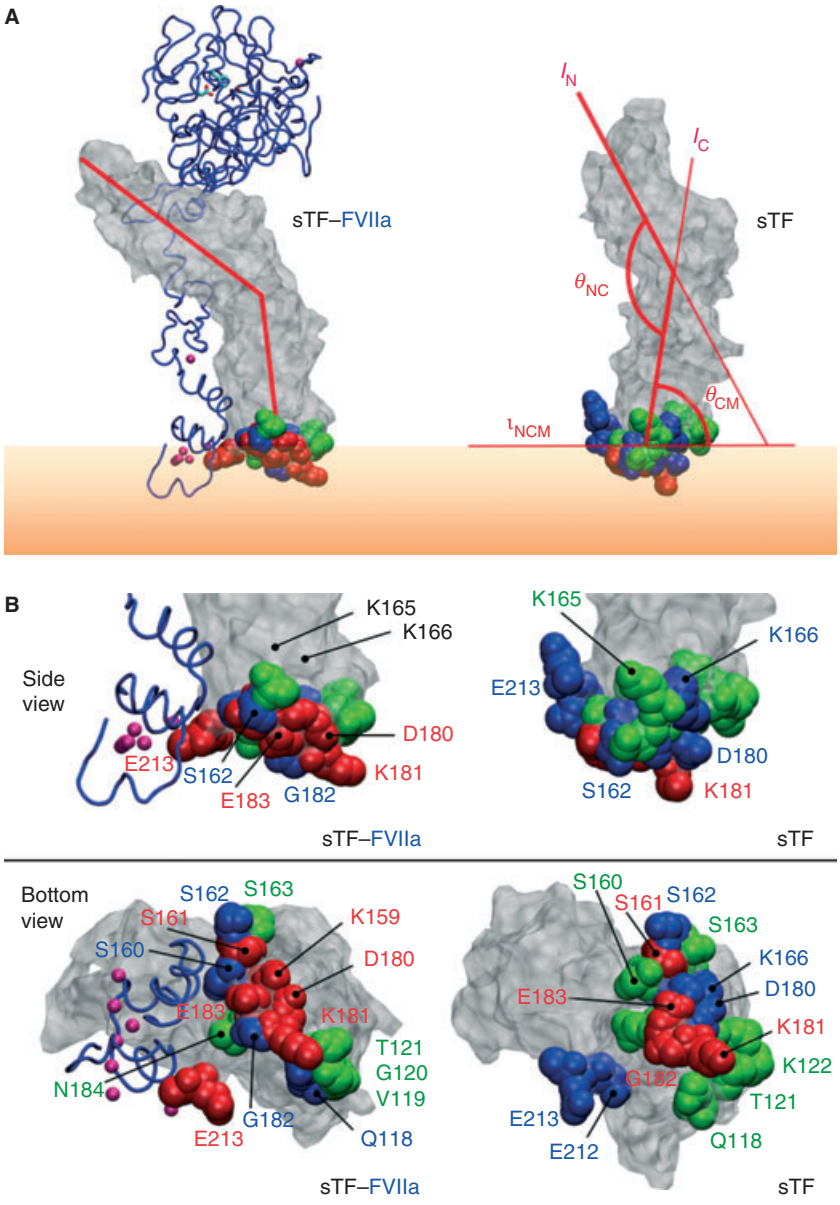


Fig. 6. Membrane orientation and lipid-interacting residues of soluble tissue factor (sTF). (A) Snapshots of membrane-bound sTF taken from the sTF–FVIIa complex (left) and isolated sTF (right) are shown. The backbone of FVIIa is drawn in blue tube representation, and sTF is drawn in gray surface representation, with the membrane-interacting residues in space-filling representations (green, blue, and red; see below for color coding). The GLA-bound calcium ions are drawn as purple spheres (not all seven ions are distinguishable in this view). Membrane-interacting residues are defined using a cut-off distance of 3.5 Å from the lipid molecules, and colored on the basis of the fraction of time for which they maintain contact with the lipid headgroups during the simulations: green for $< 30\%$, blue for 30–70%, and red for $> 70\%$. Orange shading represents the membrane. Two angles used to define the orientation of sTF (θ_{NC} and θ_{CM}) are also shown. I_N and I_C are the first two principal axes of the tissue factor (TF) N-terminal fibronectin type III domain and the TF C-terminal fibronectin type III domain, respectively, and l_{NCM} is the intersection between the plane of the membrane surface (whose normal is fixed along the z-axis) and the plane spanned by the two principal axes I_N and I_C. θ_{NC} is the angle between I_N and I_C, and θ_{CM} is that between I_C and l_{NCM}. (B) Probability of sTF residues directly interacting with the membrane. Close-up side and bottom views of snapshots shown in (A), with individual lipid-interacting residues labeled. The same color coding as in (A) has been used. Residues K165 and K166, which are strongly suspected of marking the substrate-binding side of TF [24–26,28], are also marked.

orientation of sTF on the surface of the membrane. The average and standard deviation of θ_{NC} and θ_{CM} for isolated sTF and sTF in the complex are listed in Table 4. For both angles, the standard deviation decreased slightly in the complex. As discussed above, the effect of FVIIa on the internal motion of sTF seemed to be small, thus resulting in a slight change in the average θ_{NC}, which is also evident from the overlay of the simulation snapshots shown in Fig. 2 and the Cα RMSDs listed in Table 3. However, θ_{CM} in isolated sTF was approximately 20° smaller than that of sTF in the complex, reflecting the leaning motion of sTF towards FVIIa upon complex formation. This change in orientation resulted in a different pattern of membrane interaction for sTF, specifically the change in the contact probability of residues from sTF that

© 2010 International Society on Thrombosis and Haemostasis

Table 4 Orientation of soluble tissue factor (sTF) on the membrane

System	θ_{NC} (°)	θ_{CM} (°)
sTF in sTF–FVIIa	126.6 ± 5.2	94.4 ± 4.7
sTF	132.7 ± 11.3	78.8 ± 9.8

See Fig. 6 for the definition of the two angles, θ_{NC} and θ_{CM}, used to characterize the orientation of sTF on the membrane.

directly interact with the lipid molecules. Figure 6B shows these residues, along with the fraction of the simulation time for which they maintained their contact with the lipids. Interestingly, some of the residues are proximal to the putative exosite of TF, the region that has been proposed to directly interact with the substrate (FX) [24–26,28]. Our results therefore suggest that complex formation and membrane binding might play a role in optimal presentation of the exosite region on TF, through modulating the conformation of specific regions and residues of sTF, as well as its orientation on the membrane. The direct interaction of PS headgroups with specific residues in sTF most likely also affect the conformation of these residues. Therefore, one might expect that the lipids might have an active, direct role in the decryption of sTF [49]. We are currently investigating this aspect in more detail. The GLA domain in the sTF–FVIIa complex did not change its structure or orientation against the membrane (Fig. 3A), preserving the initial Ca^{2+}–PS interactions [40]. The N-terminal residue of the GLA domain (Ala1) remained 'tucked' in the Ca^{2+}-binding region, sustaining three hydrogen bonds, with Gla20, Gln21, and Gla26, during all simulations (Fig. S1).

Concluding remarks

Unraveling the molecular mechanism(s) by which complex formation between the coagulation factors and their respective cofactors results in an immense enhancement of their enzymatic activity, and the strong dependence of such reactions on anionic membranes, hinges on atomic-resolution models of the membrane-bound forms of these complexes. In the present study, taking advantage of a crystal structure of the sTF–FVIIa complex [4] and a recent model of the membrane-bound GLA domain of FVIIa [40], we have constructed the first membrane-bound model of the binary complex of sTF and FVIIa at atomic resolution. Extensive, large-scale MD simulations have been performed to establish optimal protein–protein and protein–lipid interactions, and to investigate functionally relevant dynamic aspects of sTF and FVIIa, in their isolated form and as a complex, both in solution and on the surface of anionic membranes.

We show that FVIIa is highly dynamic in its isolated form and unlikely to provide a stable configuration for an optimal interaction with the substrate. Upon complex formation with TF, however, a significant reduction in fluctuation of FVIIa is observed in the simulations. We show that this effect results in spatial confinement, in terms of both the position and the orientation of the SP domain, and thereby the CT, not only with regard to the height of the site but also, and more dramatically, with respect to the projection of the SP domain onto the membrane.

The equilibrated membrane-bound model of the sTF–FVIIa complex also provides the first view of the orientation and relative position of sTF on the surface of a membrane. The model suggests that sTF directly interacts with the lipid headgroups, successfully accounting for experimental measurements indicating a stable orientation of sTF on the membrane [21], in a manner independent of the transmembrane region of TF or its unstructured linker. Furthermore, the model provides a framework for new experiments, for example NMR measurements or mutagenesis studies, that will examine the involvement of the specific side chains of TF in the interactions with the membrane that were identified by the simulations [50].

Acknowledgements

The authors thank C. M. Rienstra, M. A. McLean and S. Sligar for insightful discussions, and G. Enkavi for technical assistance. This work was supported by NIH grants R01-GM086749, R01-HL47014, and P41-RR05969. All the simulations were performed using the computational resources provided by TeraGrid allocation (grant number MCA06N060), primarily on the Big Red cluster at Indiana University.

Disclosure of Conflict of Interests

The authors states that they have no conflict of interest.

Supporting Information

Additional Supporting Information may be found in the online version of this article:

Fig. S1. Distance between the N-terminus of the GLA domain and its main structure.
Data S1. Supplementary material.
Video Clip S1. Dynamics of FVIIa and the sTF-FVIIa complex on the membrane.

Please note: Wiley-Blackwell are not responsible for the content or functionality of any supporting materials supplied by the authors. Any queries (other than missing material) should be directed to the corresponding author for the article.

References

1 Furie B, Furie BC. The molecular basis of blood coagulation. *Cell* 1988; **53**: 505–18.
2 Stace CL, Ktistakis NT. Phosphatidic acid- and phosphatidylserine-binding proteins. *Biochim Biophys Acta* 2006; **176**: 913–26.
3 Zwaal RFA, Comfurius P, Bevers EM. Lipid–protein interactions in blood coagulation. *Biochim Biophys Acta* 1998; **1376**: 433–53.
4 Banner DW, D'Arcy A, Chène C, Winkler FK, Guha A, Konigsberg WH, Nemerson Y. The crystal structure of the complex of blood coagulation factor VIIa with soluble tissue factor. *Nature* 1996; **380**: 41–6.

© 2010 International Society on Thrombosis and Haemostasis

5 Harvey SB, Stone MD, Martinez MB, Nelsestuen GL. Mutagenesis of the γ-carboxyglutamic acid domain of human factor VII to generate maximum enhancement of the membrane contact site. *J Biol Chem* 2003; **278**: 8363–9.

6 Nelsestuen GL. Enhancement of vitamin-K-dependent protein function by modification of the γ-carboxyglutamic acid domain: studies of protein C and factor VII. *Trends Cardiovasc Med* 1999; **9**: 162–7.

7 Huang M, Furie BC, Furie B. Crystal structure of the calcium-stabilized human factor IX Gla domain bound to a conformation-specific anti-factor IX antibody. *J Biol Chem* 2004; **279**: 14338–46.

8 Shikamoto Y, Morita T, Fujimoto Z, Mizuno H. Crystal structure of Mg^{2+}- and Ca^{2+}-bound Gla domain of factor IX complexed with binding protein. *J Biol Chem* 2003; **278**: 24090–4.

9 Mizuno H, Fujimoto Z, Atoda H, Morita T. Crystal structure of an anticoagulant protein in complex with the Gla domain of factor X. *Proc Natl Acad Sci USA* 2001; **98**: 7230–4.

10 Sabharwal AK, Padmanabhan K, Tulinsky A, Mathur A, Gorka J, Bajaj SP. Interaction of calcium with native and decarboxylated human factor X. *J Biol Chem* 1997; **272**: 22037–45.

11 Falls LA, Furie BC, Jacobs M, Furie B, Rigby AC. The ω-loop region of the human prothrombin γ-carboxyglutamic acid domain penetrates anionic phospholipid membranes. *J Biol Chem* 2001; **276**: 23895–902.

12 Huang M, Rigby AC, Morelli X, Grant MA, Huang G, Furie B, Seaton B, Furie BC. Structural basis of membrane binding by Gla domains of vitamin K-dependent proteins. *Nat Struct Biol* 2003; **10**: 751–6.

13 Ratcliffe JV, Furie B, Furie BC. The importance of specific γ-carboxyglutamic acid residues in prothrombin – evaluation by site-specific mutagenesis. *J Biol Chem* 1993; **268**: 24339–45.

14 Oganesyan V, Oganesyan N, Terzyan S, Qu D, Dauter Z, Esmon NL, Esmon CT. The crystal structure of the endothelial protein C receptor and a bound phospholipid. *J Biol Chem* 2002; **277**: 24851–4.

15 Rezende SM, Simmonds RE, Lane DA. Coagulation, inflammation, and apoptosis: different roles for protein S and the protein S–C4b binding protein complex. *Blood* 2004; **103**: 1192–201.

16 Lawson JH, Butenas S, Mann KG. The evaluation of complex-dependent alterations in human factor VIIa. *J Biol Chem* 1992; **267**: 4834–43.

17 Ruf W, Rehemtullas A, Edgington TS. Phospholipid-independent and -dependent interactions required for tissue factor receptor and cofactor function. *J Biol Chem* 1991; **266**: 2158–66.

18 Paborsky LR, Carasli IW, Fisher KL, Gorman CM. Lipid association, but not transmembrane domain, is required for tissue factor activity – substitution of the transmembrane domain with a phosphatidylinositol anchor. *J Biol Chem* 1991; **266**: 21911–16.

19 Ruf W, Kalnik MW, Lund-Hansen T, Edgington TS. Characterization of factor VII association with tissue factor in solution – high and low affinity calcium binding sites in factor VII contribute to functionally distinct interactions. *J Biol Chem* 1991; **266**: 15719–25.

20 Neuenschwander PF, Morrissey JH. Roles of the membrane-interactive regions of factor VIIa and tissue factor – the factor VIIa Gla domain is dispensable for binding to tissue factor but important for activation of factor X. *J Biol Chem* 1994; **269**: 8007–13.

21 McCallum CD, Su B, Neuenschwander PF, Morrissey JH, Johnson AE. Tissue factor positions and maintains the factor VIIa active site far above the membrane surface even in the absence of the factor VIIa Gla domain – a fluorescence resonance energy transfer study. *J Biol Chem* 1997; **272**: 30160–6.

22 McCallum CD, Hapak RC, Neuenschwander PF, Morrissey JH, Johnson AE. The location of the active site of blood coagulation factor VIIa above the membrane surface and its reorientation upon association with tissue factor. *J Biol Chem* 1996; **271**: 28168–75.

23 Morrissey JH, Neuenschwander PF, Huang Q, McCallum CD, Su B, Johnson AE. Factor VIIa–tissue factor: functional importance of protein–membrane interactions. *Thromb Haemost* 1997; **78**: 112–16.

24 Huang Q, Neuenschwander PF, Rezaie AR, Morrissey JH. Substrate recognition by tissue factor–factor VIIa – evidence for interaction of residues Lys^{165} and Lys^{166} of tissue factor with the 4-carboxyglutamate-rich domain of factor X. *J Biol Chem* 1996; **271**: 21752–7.

25 Carlsson K, Freskgård P, Persson E, Carlsson U, Svensson M. Probing the interface between factor Xa and tissue factor in the quaternary complex tissue factor–factor VIIa–factor Xa–tissue factor pathway inhibitor. *Eur J Biochem* 2003; **270**: 2576–82.

26 Kirchhofer D, Eigenbrot C, Lipari MT, Moran P, Peek M, Kelley RF. The tissue factor region that interacts with factor Xa in the activation of factor VII. *Biochemistry* 2001; **40**: 675–82.

27 Kirchhofer D, Lipari MT, Moran P, Eigenbrot C, Kelley RF. The tissue factor region that interacts with substrates factor IX and factor X. *Biochemistry* 2000; **39**: 7380–7.

28 Manithody C, Yang L, Rezaie AR. Identification of a basic region on tissue factor that interacts with the first epidermal growth factor-like domain of factor X. *Biochemistry* 2007; **46**: 3193–9.

29 Colina CM, Venkateswarlu D, Duke R, Perera L, Pedersen LG. What causes the enhancement of activity of factor VIIa by tissue factor? *J Thromb Haemost* 2006; **4**: 2726–9.

30 Hoffman M, Colina CM, McDonald AG, Arepally GM, Pedersen L, Monroe DM. Tissue factor around dermal vessels has bound factor VII in the absence of injury. *J Thromb Haemost* 2007; **5**: 1403–8.

31 Norledge BV, Petrovan RJ, Ruf W, Olson AJ. The tissue factor/factor VIIa/factor Xa complex: a model built by docking and site-directed mutagenesis. *Proteins* 2003; **53**: 640–8.

32 Venkateswarlu D, Duke R, Perera L, Darden TA, Pedersen LG. An all-atom solution-equilibrated model for human extrinsic blood coagulation complex (sTF–VIIa–Xa): a protein–protein docking and molecular dynamics refinement study. *J Thromb Haemost* 2003; **1**: 2577–88.

33 Olsen OE, Rand KD, Ostergaard H, Persson E. A combined structural dynamics approach identifies a putative switch in factor VIIa employed by tissue factor to initiate blood coagulation. *Prot Sci* 2007; **16**: 671–82.

34 Harlos K, Martin DMA, O'Brien DP, Jones EY, Stuart DI, Polikarpov I, Miller A, Tuddenham EGD, Boys CWG. Crystal structure of the extracellular region of human tissue factor. *Nature* 1994; **370**: 662–6.

35 Yves A, Muller MHU, de Vos AM. The crystal structure of the extracellular domain of human tissue factor refined to 1.7 Å resolution. *J Mol Biol* 1999; **289**: 103–12.

36 Pike ACW, Brzozowski AM, Roberts SM, Olsen OH, Persson E. Structure of human factor VIIa and its implications for the triggering of blood coagulation. *Proc Natl Acad Sci USA* 1999; **96**: 8925–30.

37 Murakami MT, Rios-Steiner J, Weaver SE, Tulinsky A, Geiger JH, Arni RK. Intermolecular interactions and characterization of the novel factor Xa exosite involved in macromolecular recognition and inhibition: crystal structure of human Gla-domainless factor Xa complexed with the anticoagulant protein NAPc2 from the hematophagous nematode Ancylostoma caninum. *J Mol Biol* 2007; **366**: 602–10.

38 Altschul SF, Gish W, Miller W, Myers EW, Lipman DJ. Basic local alignment search tool. *J Mol Biol* 1990; **215**: 403–10.

39 Morrissey JH, Pureza V, Davis-Harrison RL, Sligar SG, Ohkubo YZ, Tajkhorshid E. Blood clotting reactions on nanoscale phospholipid bilayers. *Thromb Res* 2008; **122**: S23–6.

40 Ohkubo YZ, Tajkhorshid E. Distinct structural and adhesive roles of Ca^{2+} in membrane binding of blood coagulation factors. *Structure* 2008; **16**: 72–81.

41 Phillips JC, Braun R, Wang W, Gumbart J, Tajkhorshid E, Villa E, Chipot C, Skeel RD, Kale L, Schulten K. Scalable molecular dynamics with NAMD. *J Comp Chem* 2005; **26**: 1781–802.

42 MacKerell AD Jr, Bashford D, Bellott M, Dunbrack RL Jr, Evanseck J, Field MJ, Fischer S, Gao J, Guo H, Ha S, Joseph D, Kuchnir L, Kuczera K, Lau FTK, Mattos C, Michnick S, Ngo T, Nguyen DT, Prodhom B, Reiher IWE, *et al*. All-atom empirical potential for molecular modeling and dynamics studies of proteins. *J Phys Chem B* 1998; **102**: 3586–616.

© 2010 International Society on Thrombosis and Haemostasis

43 Jorgensen WL, Chandrasekhar J, Madura JD, Impey RW, Klein ML. Comparison of simple potential functions for simulating liquid water. *J Chem Phys* 1983; **79**: 926–35.
44 Feller SE, Zhang YH, Pastor RW, Brooks BR. Constant pressure molecular dynamics simulation – the Langevin piston method. *J Chem Phys* 1995; **103**: 4613–21.
45 Martyna GJ, Tobias DJ, Klein ML. Constant pressure molecular dynamics algorithms. *J Chem Phys* 1994; **101**: 4177–89.
46 Darden T, York D, Pedersen L. Particle mesh Ewald. An N log(N) method for Ewald sums in large systems. *J Chem Phys* 1993; **98**: 10089–92.
47 Waxman E, Laws WR, Laue TM, Nemerson Y, Ross JBA. Human factor VIIa and its complex with soluble tissue factor: evaluation of asymmetry and conformational dynamics by ultracentrifugation and fluorescence anisotropy decay methods. *Biochemistry* 1993; **32**: 3005–12.
48 Wang Y, Ohkubo YZ, Tajkhorshid E. Gas conduction of lipid bilayers and membrane channels. In: Feller S, ed. *Current Topics in Membranes: Computational Modeling of Membrane Bilayers*, Oxford: Elsevier, 2008: 343–67.
49 Bach RR. Tissue factor encryption. *Arterioscler Thromb Vasc Biol* 2006; **26**: 456–61.
50 Morrissey JH, Pureza V, Davis-Harrison RL, Sligar SG, Rienstra CM, Kijak AZ, Ohkubo YZ, Tajkhorshid E. Protein–membrane interactions: blood clotting on nanoscale bilayers. *J Thromb Haemost* 2009; **7**(S1): 169–72.

© 2010 International Society on Thrombosis and Haemostasis